Electromagnetic wave sensors

Effects of Barrier Energy Offset and Gradient in Extended Wavelength Infrared Detectors

Dilip Chauhan[1*], A. G. Unil Perera[1**], Lianhe Li[2], Li Chen[2], and Edmund H. Linfield[2]

[1] Center for Nano-Optics, Department of Physics and Astronomy, Georgia State University, Atlanta, GA 30303 USA
[2] School of Electronic and Electrical Engineering, University of Leeds, Leeds LS2 9JT, U. K.
* Student Member, IEEE
** Fellow, IEEE

Manuscript received August 15, 2018; revised October 12, 2018; accepted November 9, 2018. Date of publication November 12, 2018; date of current version November 29, 2018.

Abstract— The extended wavelength infrared (IR) photodetectors are the new class of III-V semiconductor heterojunction-based photodetectors that can detect incoming radiation with energy significantly smaller than the minimum energy gap (Δ) at the heterojunction interface. The architecture of these photodetectors includes a barrier-emitter-barrier epilayers sandwiched between highly doped ohmic top and bottom contact layers. An energy offset (δE) between the barriers is necessary for the extended wavelength photodetection. In this article, we study the performance of extended wavelength IR photodetectors with varying δE and gradient of the potential barrier. Results indicate that the extended wavelength threshold varied slightly with varying both the gradient and offset. Spectral responsivity, however, increased with the increasing offset and decreased with increasing gradient.

Index Terms—Electromagnetic wave sensors, extended wavelength infrared (IR) photodetectors, GaAs/AlGaAs heterostructures, III-V semiconductors.

I. INTRODUCTION

Extended wavelength infrared (IR) photodetectors have been explored as a novel way of developing IR detectors capable of detecting the IR radiation of an energy much smaller than the minimum energy gap (Δ) of the absorbing material, or the interfacial energy gap of the heterostructure [1]–[3]. In conventional photodetectors, wavelength threshold (λ_t) of the spectral photoresponse is given by the relation $\lambda_t = hc/\Delta$ [4]. In heterostructure-based IR detectors such as p-GaAs/ $Al_xGa_{1-x}As$ IR detectors, the Δ is the interfacial energy gap, given as the difference between the Fermi level at equilibrium in the p-GaAs layer and the potential barrier energy in the $Al_xGa_{1-x}As$ layer. λ_t can be tuned by changing the Al mole fraction x. The p-GaAs/ $Al_xGa_{1-x}As$ IR detectors have been studied for the spectral ranges spanning mid-wave IR to the very-long-wave IR (VLWIR) range [5], [6]. A p-type doped GaAs layer absorbs IR radiation due to intravalence band transitions [7], i.e., from light-hole (L-H)/heavy-hole (H-H) bands to split-off (S-O) band and H-H to L-H band, where the energy gap between the valence band edge and the S-O band (Δ_{SO}) is 0.34 eV [see Fig. 1(b)]. The S-O band photoresponse is dominant for wavelength shorter than $\sim$3.5 μm and H-H/L-H band photoresponse can be observed beyond 3.5 μm, up to $\sim$10 μm range [7]. Free-carrier absorption also occurs, which becomes stronger [8] at longer wavelengths as λ^2. In the conventional approach, the spectral region of photoresponse, and hence, λ_t is determined by the Δ, which is also the minimum energy required for internal photoemission at the heterojunction. However, in the extended wavelength IR detectors, λ_t is not limited by Δ. The photo-excited carriers (or the hot-carriers) give rise to a quasi-Fermi level at a higher energy state than in the equilibrium condition [9], thereby lowering the effective Δ, thus forming the basis for extended wavelength IR detection. Hot-carrier related mechanisms have been studied due to interesting applications in photo-detection and solar energy conversion [9]–[11]. In the extended wavelength IR detector reported recently, a λ_t $\sim$60 μm was observed owing to the wavelength extension mechanism in a p-GaAs/ $Al_xGa_{1-x}As$ IR detector, which would otherwise have a conventional λ_t $\sim$3.1 μm (3). Whilst the wavelength extension mechanism enabled a spectral photoresponse with λ_t $\sim$60 μm, the dark current was found to be determined by the $\Delta(\sim 0.40$ eV) corresponding to $\lambda_t \sim 3.1$ μm. The

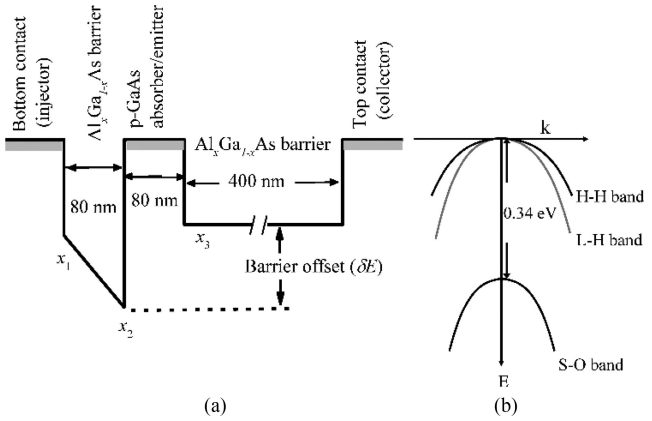

Fig. 1. Schematic diagram of the valence band alignment of the detectors in equilibrium consists of an emitter (80 nm), an $Al_xGa_{1-x}As$ barrier (80 nm) at the bottom graded by tuning the Al mole fraction from x_1 to x_2, and a 400-nm $Al_xGa_{1-x}As$ barrier at the top; thus, an energy offset (δE) has been set up between the two barriers. The detail parameters of five devices are shown in Table 1.

Corresponding author: A. G. U. Perera (e-mail: uperera@gsu.edu).
Associate Editor: M. Rinaldi.
Digital Object Identifier 10.1109/LSENS.2018.2881047

Table 1. Device Parameters of the Samples With Varying Barrier Energy Offset (δE) Between, and Gradient.

Sample	Graded Barrier x_1	x_2	Gradient (kV/cm)	Constant barrier x_3	Offset (δE) (eV)
SP1007	0.45	0.75	20.6	0.57	0.10
15SP3	0.45	0.75	20.6	0.39	0.19
GSU17I	0.45	0.75	20.6	0.30	0.23
GSU17II	0.33	0.75	28.9	0.39	0.19
GSUIII	0.21	0.75	37.1	0.39	0.19

detector architecture consists of barrier-emitter(absorber)-barrier layers sandwiched between highly doped contact layers that also serve as injector and collector. The valence band alignment under an equilibrium for a typical p-GaAs/ $Al_xGa_{1-x}As$ heterostructure-based IR detector, with a barrier energy offset (δE) is shown schematically in Fig. 1(a). It has been found that the fundamental requirement for the wavelength extension mechanism is the barrier energy offset [1]. Without the offset (i.e., when $\delta E = 0$ eV), the spectral photoresponse agrees well (2) with the conventional limit of Δ. The $Al_xGa_{1-x}As$ barrier on the injector side was linearly graded by tuning x in the growth direction. The graded barrier was expected to improve the carrier injection to the emitter [12] and was also found to be more efficient for wavelength extension mechanism compared to a constant barrier [2]. Given these observations, understanding the effects of energy offset, and gradient of the barrier is critical to optimize the operation of IR detectors based on a wavelength extension mechanism.

In this article, we present the results of an experimental study of extended wavelength IR detectors with varying energy offset (with gradient unchanged), and varying gradient (with energy offset unchanged). The results indicate that the spectral responsivity increased with increasing offset, whilst the effect was opposite in case of increasing gradient. However, the extended wavelength threshold did not show a significant variation in both cases.

II. EXPERIMENTAL

A. Device Design, Growth, and Mesa Processing

Five p-GaAs/$Al_xGa_{1-x}As$ heterostructure-based IR detectors (SP1007, 15SP3, GSI17I, GSU17II, GSU17III) were used in this study. Design parameters for each device are summarized in Table 1. These devices were grown by molecular beam epitaxy (MBE) [13] on a semi-insulating GaAs substrate. The active region of the photodetector consists of a graded $Al_xGa_{1-x}As$ barrier, followed by a p-GaAs emitter, and then, another constant $Al_xGa_{1-x}As$ barrier. These emitter/barrier layers are sandwiched between the bottom and top contact layers of p-type doped GaAs, with thicknesses of 0.5 and 0.2 μm, respectively. The emitters, and the top and bottom contact layers, are degenerately doped at 1×10^{19} cm^{-3} that leads the equilibrium Fermi level to align slightly below the valence band edge. The graded and constant barriers are 80 and 400 nm, respectively, whilst the p-GaAs emitter is 80 nm in all devices. The energy offset (δE) is set up due

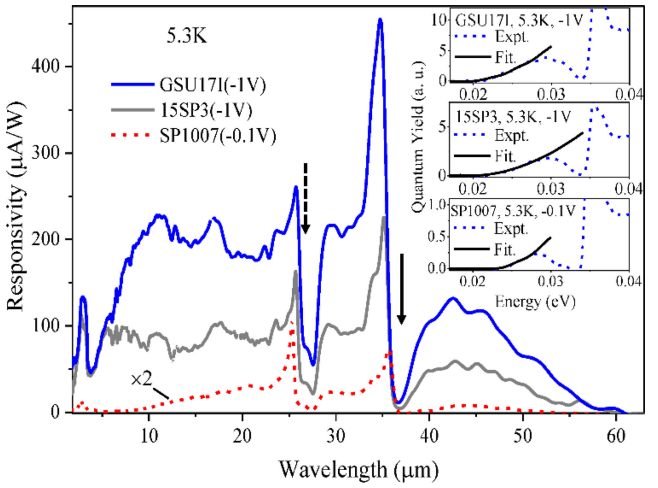

Fig. 2. Responsivity of the samples increased with increasing offset. There is no significant effect of the offset to the wavelength threshold. The inset shows the TDIPS fittings to obtain the wavelength threshold. The dashed and solid arrows indicate the AlAs- and GaAs-like phonons absorption features, respectively.

to the difference in the barrier potential energy of two barriers. The graded barrier profile is obtained by linearly varying the Al mole fraction (x) from x_1 to x_2 along the growth direction. Out of the five devices, SP1007, 15SP3, and GSU17I constitute a set with the varying offsets, whilst 15SP3, GSU17II, and GSU17III constitute another set with varying gradients. Square shaped mesas were fabricated by conventional photolithography and wet etching, followed by Ti/Pt/Au metallization and lift-off to form contact electrodes. Each mesa has anelectrically active area of 400 $\times$ 400 μm^2. The top contact layer (p-GaAs) was partially etched to open an optical window of $\sim$260 $\times$ 260 μm^2 for normal incidence optical illumination of the detector. The mesas were wire bonded to a chip carrier for experimental studies.

B. Characterization

Current–voltage characteristics were measured using a Keithley 2400 source meter. A positive bias on the device refers to a positive voltage connected to the top contact, with the bottom contact grounded. Similarly, a negative bias refers to the positive voltage connected to the bottom contact, with the top contact grounded. A spectral photoresponse was measured at using a Fourier transform IR spectrometer and calibrated using a commercial Si composite bolometer to measure the background intensity.

III. RESULTS AND DISCUSSION

The photoresponse of the three detectors with the increasing offset ($\delta E = 0.10, 0.19$, and 0.23 eV for SP1007, 15SP3, and GSU17I, respectively) are shown in Fig. 2. The AlAs- and GaAs-like phonon features [1] are shown by dashed and solid arrows, respectively. The sharp peaks near 25.5 and 35.6 μm due to strong plasmon–phonon coupling modes, are consistent with the previously observed results in [1]. The responsivity for 15SP3 and GSU17I are presented for -1V, whereas for SP1007, it is presented for –0.1 V. These bias values correspond to the optimum performance of photoresponse measured in

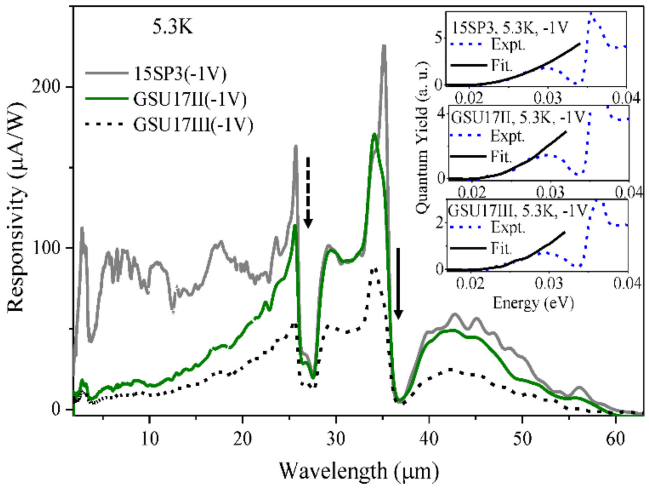

Fig. 3. Responsivity of three samples decreases with increasing gradient but there is no significant effect of the gradient on the wavelength threshold. The inset shows the TDIPS fittings to obtain the wavelength threshold. The dashed and solid arrows indicate the AlAs- and GaAs-like phonons absorption features, respectively.

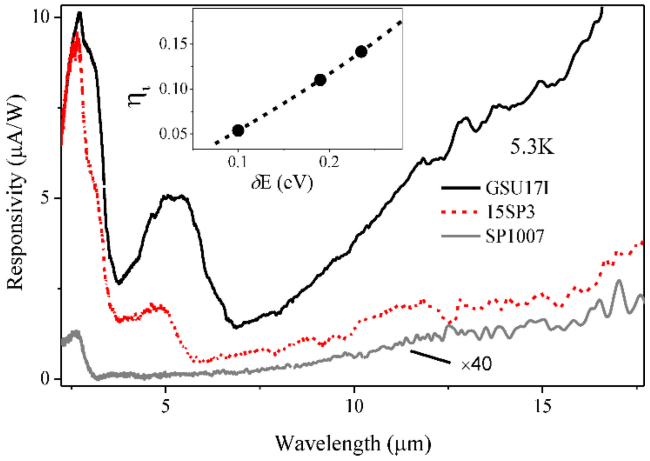

Fig. 4. Photoresponse of the three detectors with increasing offset, at zero bias. The photoresponse increases with increasing offset. The inset shows the internal photoemission efficiency (η) as a function of the offset. The solid dots represent the three devices.

each device. A lower value of the optimum bias voltage in SP1007 can be understood in terms of nonuniform voltage drop across the two barriers due to the difference their dc resistances [5], [14]. At a low bias, voltage-drop across the bottom graded barrier will be larger. But, increasing bias causes its dynamic resistance to lower; then, the bias distribution across both barriers approaches more uniformity. When this condition is reached, the photo-excited carriers in the emitter are severely swept out disabling the quasi-Fermi level distribution. Hence, the extended wavelength photoresponse at further high biases (higher than ~ –0.2 V) disappears in SP1007, as reported previously [1]. The higher offset in 15SP3 and GSU17I is equivalent to lower top barrier, which then needs an even larger bias to reach an uniformity in the bias distribution. Therefore, 15SP3 and GSU17I showed the extended wavelength photoresponse at higher applied biases compared to SP1007. Note that the responsivity of SP1007 is shown with a two-fold multiplication for better readability. The results clearly show that the responsivity increased with increasing the value of offset. A temperature-dependent internal photoemission spectroscopy (TDIPS) method [15] was employed to determine the energy (Δ') corresponding to the spectral threshold of the photoresponse. In this method, Δ' is obtained as the fitting parameter to fit the quantum yield ($Y(h\nu) \sim (h\nu - \Delta')^2$) near-threshold region. Thus, the values of the λ_t were found to be ~56, 60, and 61 μm, respectively, for SP1007, 15SP3, and GSU17I as determined from TDIPS fitting (see inset, Fig. 2). Similarly, the photoresponse of the detectors with increasing gradients (20.6, 28.9, and 37.1 kV/cm under equilibrium for 15SP3, GSU17II, and GSU17III, respectively) are shown in Fig. 3. The responsivity of all three samples are presented at –1 V. The values of the λ_t obtained by TDIPS fitting (inset, Fig. 3) were found to be ~60, 57, and 58 μm for 15SP3, GSU17II, and GSU17III, respectively. The responsivity was found to suggest a decreasing pattern with the increasing gradient for the three devices.

These results indicate that the wavelength threshold of the photoresponse does not vary significantly with increasing the offset and the gradient. However, the responsivity shows a pattern of increasing responsivity with the offset although it decreases with increasing gradient. The increased offset is the result of the decreased barrier energy of the constant barrier since the graded barrier energy is constant in all devices. At the emitter/barrier interface, the internal photoemission quantum efficiency η_i is proportional to $[\frac{2}{3}\{(E_F + h\nu)^{\frac{3}{2}} - (E_F + \Delta'')^{\frac{3}{2}}\} - (h\nu - \Delta'')(E_F + \Delta'')^{\frac{1}{2}}]/[(E_F + h\nu)^{\frac{3}{2}} - (h\nu)^{\frac{3}{2}}]$, where E_F is the Fermi level, and Δ'' is the energy gap at the emitter/collector barrier interface [16]. The barrier offset is given as $\delta E = \Delta - \Delta''$, where Δ is constant for all devices. Thus, the η is expected to increase with the increasing δE. In fact, the photoresponse confirms the pattern of increasing responsivity also at a zero bias, as shown in Fig. 4. The wavelength threshold at zero bias closely agrees with Δ ~0.4 eV (~3.1 μm), at the high temperature of ~100 K, when the extended wavelength mechanism dissapears [3]. However, at the very low tempreatures (5.3 K), the extended wavelength mechanism is also observed at zero bias. In the absence of any effect of applied bias, the zero bias photoresponse arises due to the internal photoemission followed by the collection at the contacts. Note that the photo-excitation occurs at top contact, emitter, and the bottom contact simultaneously, but the collection efficiency [16] is given as $\eta_c = \exp(-z_m/L_s)$, where z_m is the position of barrier maximum, and L_s is carrier scattering length and determines the net carrier flow. Due to the graded barrier, $\eta_c \sim 1$ for the carrier flow from the emitter to the bottom contact (since $z_m \sim 0$), but $\eta_c \ll 1$ for the carrier flow from the bottom contact to the emitter. Thus, the graded barrier will cause a net carrier flow at zero bias, from the emitter to the bottom contact. The internal photoemission from the top contact over the constant barrier is important to maintain the carrier flow. Therefore, the lower magnitude of Δ'' is expected to increase the η_i and, hence, the photoresponse at zero bias. The inset in Fig. 4 shows an increasing pattern of η_i with δE evaluated for arbitrary energy $h\nu$ corresponding to 2.7 μm, where the solid dots represent the three devices with increasing δE. The increasing photoresponse with increasing offset can be attributed the increasing η_i due to lowering of Δ'', even though a precise empirical connection cannot be

established. On the other hand, the decreasing photoresponse with the increasing gradient is not fully understood. Yet, it can be suggested that a moderate or low value of the gradient is more suitable for the extended wavelength photoresponse.

The results from this study are significant towards the deeper understanding of the extended wavelength photoresponse mechanism in terms of the effect of the heterostructure parameters despite the relatively weak responsivity. From the technological point of view, the MBE growth capability and mature III-V material system can enable high flexibility in design parameters. The detector optimization may also need further study in effect of the barrier thickness (possibly less than 400 nm used in this study) on carrier transport, given the low carrier energy from VLWIR absorption. Quantum nanostructures such as dots-in-a-well IR detectors may also be explored for the extended wavelength mechanism due to their long carrier lifetime [17].

IV. CONCLUSION

The experimental study of the extended wavelength IR photodetectors has been carried out by varying the barrier energy offset and gradient of the graded barrier. The results indicated that the increasing offset improves the internal photoemission efficiency at the emitter/collector barrier interface, leading to higher photoresponse. An increasing gradient caused the photoresponse to decrease, however. The wavelength threshold did not show a significant variation in both cases. These results are expected to be useful for design optimization of the extended wavelength IR photodetector.

ACKNOWLEDGMENT

This work was supported in part by the U.S. Army Research Office under Grant W911 NF-15-1-0018; in part by the National Science Foundation under Grant ECCS-1232184; and in part by the European Community's Seventh Framework Programme (FP7-IDEAS-ERC) under Grant 247375 "TOSCA," The work of D. Chauhan and E. Linfield was supported by the GSU Brains and Behavior Fellowship and the Royal Society and Wolfson Foundation, respectively.

REFERENCES

[1] Y.-F. Lao, A. G. U. Perera, L. H. Li, S. P. Khanna, E. H. Linfield, and H. C. Liu, "Tunable hot-carrier photodetection beyond the bandgap spectral limit," *Nat. Photon.*, vol. 8, pp. 412–418, 2014.

[2] D. Chauhan, A. G. U. Perera, L. Li, L. Chen, S. P. Khanna, and E. H. Linfield, "Extended wavelength infrared photodetectors," *Opt. Eng.*, vol. 56, 2017, Art. no. 091605.

[3] D. Chauhan, A. G. U. Perera, L. H. Li, L. Chen, and E. H. Linfield, "Dark current and photoresponse characteristics of extended wavelength infrared photodetectors," *J. Appl. Phys.*, vol. 122, 2017, Art. no. 024501.

[4] S. M. Sze and K. K. Ng, *Physics of Semiconductor Devices*, 3rd ed. Hoboken, NJ, USA: Wiley-Interscience, 2007.

[5] D. Chauhan, A. G. U. Perera, L. H. Li, L. Chen, and E. H. Linfield, "Effect of a current blocking barrier on a 2–6 μm p-GaAs/AlGaAs heterojunction infrared detector," *Appl. Phys. Lett.*, vol. 108, 2016, Art. no. 201105.

[6] D. G. Esaev, M. B. M. Rinzan, S. G. Matsik, and A. G. U. Perera, "Design and optimization of GaAs/AlGaAs heterojunction infrared detectors," *J. Appl. Phys.*, vol. 96, pp. 4588–4597, 2004.

[7] Y. F. Lao *et al.*, "Light-hole and heavy-hole transitions for high-temperature long-wavelength infrared detection," *Appl. Phys. Lett.*, vol. 97, 2010, Art. no. 091104.

[8] A. L. Korotkov *et al.*, "Free-carrier absorption in Be- and C-doped GaAs epilayers and far infrared detector applications," *J. Appl. Phys.*, vol. 89, pp. 3295–3300, 2001.

[9] M. L. Brongersma, N. J. Halas, and P. Nordlander, "Plasmon-induced hot carrier science and technology," *Nat. Nano*, vol. 10, pp. 25–34, 2015.

[10] N. M. Gabor *et al.*, "Hot carrier–assisted intrinsic photoresponse in graphene," *Science*, vol. 334, pp. 648–652, 2011.

[11] M. Freitag, T. Low, F. Xia, and P. Avouris, "Photoconductivity of biased graphene," *Nat. Photon.*, vol. 7, pp. 53–59, 2013.

[12] S. G. Matsik, P. V. V. Jayaweera, A. G. U. Perera, K. K. Choi, and P. Wijewarnasuriya, "Device modeling for split-off band detectors," *J. Appl. Phys.*, vol. 106, 2009, Art. no. 064503.

[13] L. H. Li, J. X. Zhu, L. Chen, A. G. Davies, and E. H. Linfield, "The MBE growth and optimization of high performance terahertz frequency quantum cascade lasers," *Opt. Exp.*, vol. 23, pp. 2720–2729, 2015.

[14] H. C. Liu, J. Li, J. R. Thompson, Z. R. Wasilewski, M. Buchanan, and J. G. Simmons, "Multicolor voltage tunable quantum-well infrared photodetector," *IEEE Trans. Electron. Devices*, vol. 40, no. 11, Nov. 1993, Art. no. 2142.

[15] Y.-F. Lao and A. G. U. Perera, "Temperature-dependent internal photoemission probe for band parameters," *Phys. Rev. B*, vol. 86, 2012, Art. no. 195315.

[16] A. G. U. Perera, H. X. Yuan, and M. H. Francombe, "Homojunction internal photoemission far-infrared detectors: Photoresponse performance analysis," *J. Appl. Phys.*, vol. 77, pp. 915–924, 1995.

[17] S. Wolde *et al.*, "High temperature terahertz response in a p-type quantum dot-in-well photodetector," *Appl. Phys. Lett.*, vol. 105, 2014, Art. no. 151107.